

Emission Spectrum of Doped Graphene Quantum Dots: A high-throughput TDDFT Analysis

Mustafa Coşkun Özdemir

Department of Chemistry, İzmir Institute of Technology, İzmir, Türkiye

Caner Ünlü

Department of Chemistry, İstanbul Technical University, İstanbul, Türkiye

Şener Özönder

*Institute for Data Science & Artificial Intelligence, Boğaziçi University, İstanbul, Türkiye**

We present time-dependent density functional theory (TDDFT) calculations of fluorescence emission energies for 284 distinct graphene quantum dots (GQDs) of varying shapes (square, hexagonal, and amorphous) and sizes ($\sim 1-2$ nm). These GQDs are doped with one or two elements from B, N, O, S, and P at dopant percentages of 1.5%, 3%, 5%, and 7%. Our study systematically investigates the trends and patterns in emission energies as a function of shape, size, dopant type and dopant percentage. Twelve structures are identified to have emission wavelengths in the visible spectrum. The emission energies derived from our calculations can guide the formulation of specific GQD mixtures to achieve desired emission spectra within and beyond the visible range for industrial applications. Furthermore, the extensive dataset, including emission energies along with molecular structures generated in this work, creates a DFT dataset for further machine learning studies.

* Corresponding author: sener.ozonder@bogazici.edu.tr

I. INTRODUCTION

Graphene quantum dots (GQDs) are carbon-based 2D nanomaterials which consist of sp^2 hybridized carbon atoms with lateral dimensions typically less than 10 nm, displaying unique electronic, optical, and chemical properties due to quantum confinement and edge effects [1–6]. These carbon-based 2D nanomaterials exhibit exceptional photoluminescence, high surface area and biocompatibility, making them ideal candidates for various applications in bioimaging, sensing, and optoelectronics [7–18].

GQDs have become center of attention in recent years due to their tunable fluorescence properties, which can be controlled by altering their size, shape, composition and functional groups, facilitating their use in advanced light-emitting devices, solar cells and photodetectors [7, 8]. Two primary pathways contribute to the fluorescence of GQDs: intrinsic state emission, which is associated with the sp^2 -hybridized carbon core, and surface state emission, which is influenced by the surface chemical groups and carbon bonds [19]. The combination of surface defects, functional groups, and heteroatom doping in the core of GQDs greatly affects their fluorescence properties [19]. Additionally, surface alterations like oxidation and reduction can adjust the colors of their emissions [19–21].

Experimental research on heteroatom doped graphene quantum dots has shown that doping distinct atoms to GDQs can control a variety of optical properties of the dots, including photoluminescence wavelength and quantum yield. The photophysical properties of GQDs undergo significant changes when doped with N and B atoms such as increasing their quantum yield and resulting in controllable shifts in their emission wavelength [22–24]. It was demonstrated that the photoluminescence of GQDs can be enhanced by doubly doping them with Mg and N [24]. It was also shown that doping GQDs with S, N, and B resulted in red light emission [22]. In a separate recent study, doping GQDs with N and P or B can create dual emission spectrum [25, 26].

Enhanced photoluminescence, improved photostability and tailored electronic properties can be obtained with heteroatom-doped GQDs. These can in turn result in important breakthroughs in bioimaging, energy storage, optoelectronics, environmental monitoring and other fields [27–30].

Time-dependent density functional theory (TDDFT) has been successfully applied to calculate excitation energies, optical absorption and emission spectra, and electronic transition properties of molecular systems. It offers a compelling alternative to computationally demanding, highly correlated *ab initio* methods for investigating the electronic structure and optical properties of molecular systems [31–33]. By extending the principles of ground-state density functional theory

(DFT) to the time domain, TDDFT achieves this while maintaining acceptable accuracy at a lower computational cost. The versatility and efficiency of TDDFT have made it a particularly attractive approach for studying the unique characteristics of GQDs. Numerous studies have utilized TDDFT to investigate the optical properties of GQDs, exploring topics such as the impact of nitrogen dopant configuration [21], the utilization of enhanced light absorption [34], the influence of edge modifications[35] and more [20, 36–39].

The TDDFT literature usually consists of studies concerning few particular types of GQDs and these fragmented studies do not reveal the systematics of the effect of shape, size and dopants on the emission spectrum of GQDs. In this work, we conduct a high-throughput TDDFT calculations aiming to investigate the effect of shape, size, (co-)dopant type and dopant percentage on the emission spectrum of 284 distinct GQDs. The systematics and trends to be learned from this analysis can be used as a guide for design engineering desired emission spectra for various applications and concurrently reducing the number of trial-and-errors during synthesis.

II. COMPUTATIONAL DETAILS

Fluorescence emission energies from S1→S0 for square, hexagonal, and amorphous-shaped GQDs have been calculated. The ten structures considered are shown in Fig. 1. These pristine GQDs and their singly-doped (B, O, P, S, N) and doubly-doped variants (BO, OS, BP, BS, NO, NS, BN, NP, OP, SP) at dopant percentages of 1.5%, 3%, 5% and 7% constitute a total of 610 GQDs. This large sample size extensively covers the chemical space of GQDs with sizes of approximately ~1-2 nm.

Amorphous-shaped GQDs structurally interpolating hexagonal and square shapes are derived from 1 nm square structures to examine the effect of structural defects on the emission spectrum. Furthermore, the amorphous structures facilitate the investigation of the effects on the emission energies caused by the breaking of symmetries present in hexagonal and square structures. Symmetric structures contain degenerate states that affect the HOMO-LUMO gap, hence, symmetry breaking is of immense effect on the emission energies.

Hydrogen atoms are added to the edges of the molecules to passivate the dangling bonds. All structures are ensured to be neutral in charge and have zero total spin; an extra dopant or hydrogen atom is added to or removed from some structures to achieve this. The reported dopant percentages are defined as the percentage of dopant atoms relative to all atoms excluding hydrogens.

Geometries have been pre-optimized using the Semiempirical Extended Tight-Binding Program

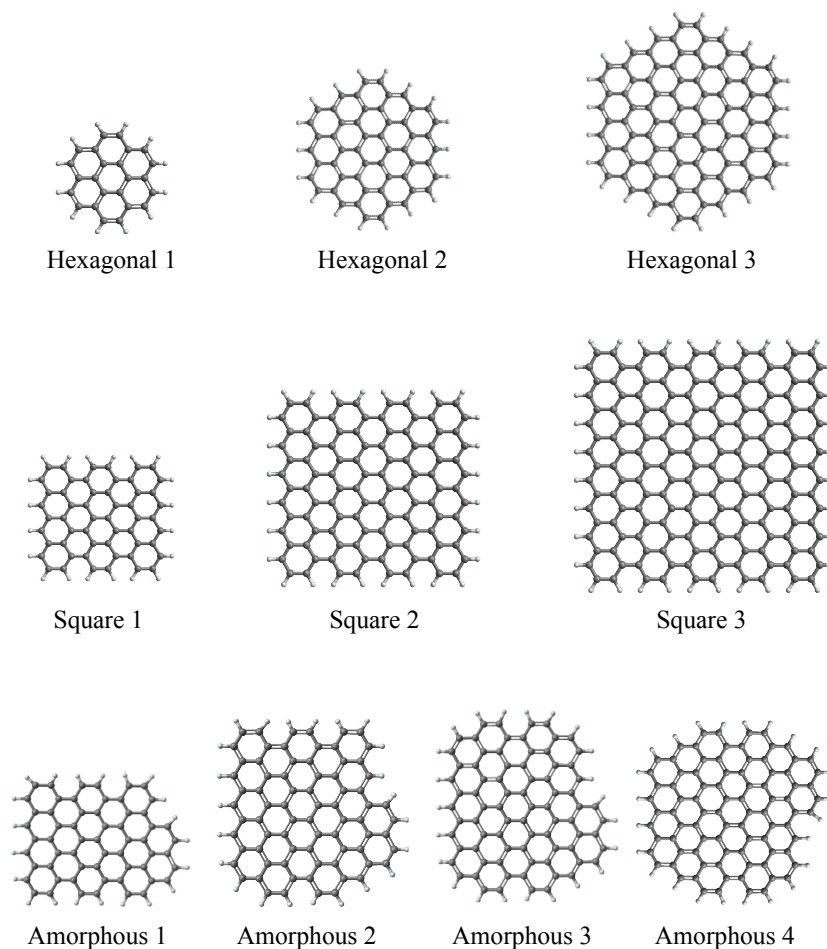


Figure 1. The structures along with their singly- and doubly-doped variants were used to calculate emission energies via TDDFT. The square shapes have 1 nm, 1.5 nm and 2 nm side lengths.

Package [40] at the Bannwarth2019-xTB [41] level of theory to reduce the initial computational cost. Ground state (S_0) and excited state (S_1) optimizations have been performed with Gaussian16 [42] using the hybrid functional B3LYP [43–45] and the basis set 6-31G(d) [46–52]. Both DFT for geometry optimization and TDDFT for excited state calculations are performed in water within the framework of the polarizable continuum model (PCM) [43, 53]. Both of the optimized S_0 and S_1 states have been verified by frequency analysis to be free from imaginary frequencies.

Structures that did not converge, were not optimized or had virtual frequencies have not been re-run and consequently not reported, as they would require manual intervention, which in turn impedes the streamlined workflow of high-throughput screening. This yielded 284 successful TDDFT results out of 610 possible structures. All calculations were done with 128-core nodes and the total wall time for the entire calculations reported here is 6223 node-hours, producing approximately 1.7

TB of checkpoint files.

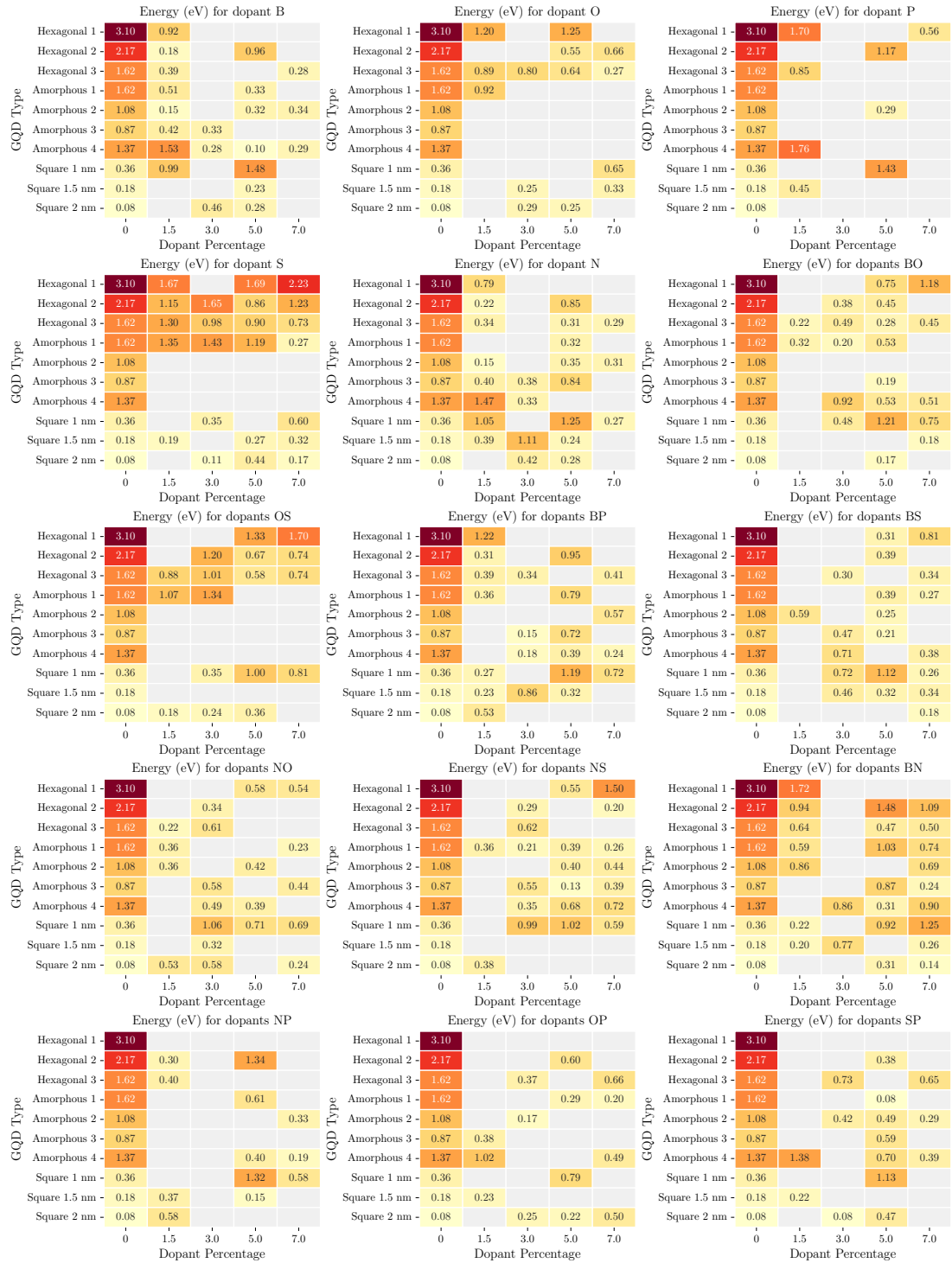


Figure 2. Emission energies in eV of 284 GDQs are presented where each heatmap panel for a different single or double dopants. Missing slots belong to the structures that did not converge, were not optimized or had virtual frequencies.

III. RESULTS AND DISCUSSION

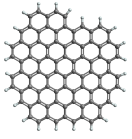
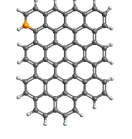
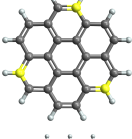
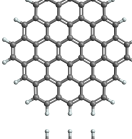
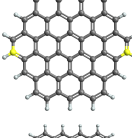
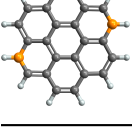
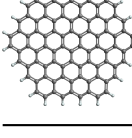
The electronic structure of GQDs and accordingly their emission energies and intensities (oscillator strength) vary strongly depending on the nanocrystal's shape, size, dopant type and dopant percentage. In this work, the emission energies of 284 different structures were found using TDDFT excited-state calculations. All emission energies in eV are summarized in Fig. 2, where each heatmap panel belongs to a different dopant atom(s). According to the Kasha's rule, fluorescence emission can only occur from the lowest energy state of S1 state. The energies reported in Fig. 2 corresponds to S1→S0 transitions. Possible phosphorescence phenomenon which involves triplet states have not been investigated in this study.

As revealed in Fig. 2, for the pristine hexagonal and square structures, the emission energy decreases with increasing structure size as expected due to quantum confinement. As the structure size grows, its HOMO-LUMO gap closes, causing the photoluminescence spectrum to shift towards the IR region. This trend is somewhat preserved for the doped hexagonal and square structures. Amorphous structures were specifically prepared to be a transitional form between square and hexagonal ones to check if their energies interpolate between those of square and hexagonal structures. This indeed can be seen from Fig. 2.

Hexagonal 2 C₅₄H₁₈ and Square 1 C₅₄H₂₀ have the same number of carbon atoms. Hexagonal 3 C₉₆H₂₄ and Square 2 C₁₀₄H₂₈ also have a similar number of atoms. However, these structure have stark differences in terms of emission energy. This can be attributed to the fact that they have different symmetry properties. The pristine square structure has D_{4h} point group symmetry, while the pristine hexagonal structure has D_{6h} point group symmetry. The amount of degeneracy in orbital energies affects the HOMO and LUMO energies, as well as the gap between them. This can be related to the particle in a 2D square and circular box toy models from introductory quantum mechanics. In a 2D box, energy depends on the quantum numbers as $E \propto n_x^2 + n_y^2$, where $n_x = n_y$ in the square box case, which in turn brings degeneracy. In a circular box, quantum numbers are x_{mn} , which is the n -th zero of the m -th Bessel function J_m . So, despite having the same or similar atomic content, different symmetries of shapes yield different emission energies.

When we specifically examine the direct effects of dopants on hexagonal and amorphous structures (Fig. 2), we find that sulfur as the dopant usually leads to the highest emission energies. Sulfur, by providing extra valence electrons in the $3s^23p^4$ orbitals, facilitates N-type doping on the carbon surface. Although sulfur and oxygen have the same number of valence electrons, the valence electrons of oxygen are located in the second shell and do not result in high emission energies unlike

Table I. Structures with emission energy in the visible region. Dopant colors are P (orange), B(pink), N (blue), O (red) and S (yellow).

Structure	Energy (eV)	Wavelength		Dopants (%)	Structure	Energy (eV)	Wavelength		Dopants (%)
		(nm)					(nm)		
	1.62	763		pristine		1.67	740		S (1.5%)
	1.76	705		P (1.5%)		1.69	734		S (5%)
	3.10	399		pristine		2.23	556		S (7%)
	1.72	722		BN (1.5%)		2.17	572		pristine
	1.70	728		OS (7%)		1.65	750		S (3%)
	1.70	728		P (1.5%)		1.62	767		pristine

in the case of sulfur. Additionally, doping with oxygen or codoping with oxygen and sulfur atoms yields similar results. We also observe that sulfur-doped structures predominantly have emission energies above 1 eV. The calculated emission energies range between 0.08 and 3.10 eV. Table I shows the only 12 structures that emit light in the visible electromagnetic spectrum whereas the majority of GQD structures emit in the infrared (IR) region.

Figure 3 shows the energy and oscillator strength of the 284 structures, categorized into groups of square, hexagonal, and amorphous. Most emission energies are in the infrared range or beyond, while some fall within the visible range (1.6-3.3 eV or 380-750 nm). A few hexagonal structures are found to have emission energies exceeding 1.5 eV.

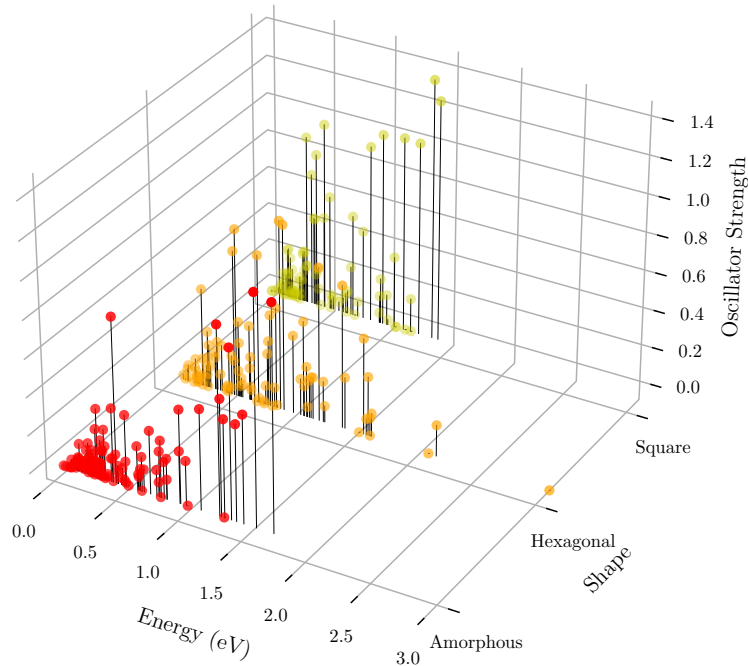


Figure 3. Oscillator strength of 284 GQDs with respect to their shape and emission energies as calculated from TDDFT.

IV. CONCLUSIONS AND OUTLOOK

In this study, we performed an extensive high-throughput TDDFT analysis to investigate the emission spectra of 284 distinct graphene quantum dots (GQDs) of various shapes, sizes, and dopant configurations. Our results highlight the intricate dependence of emission energies on the structural characteristics and doping patterns of GQDs. The findings reveal that the emission energies generally decrease with increasing GQD size due to quantum confinement effects, while specific dopants, particularly sulfur, significantly influence the emission properties, often leading to higher emission energies.

Among the structures studied, only a select few exhibited emission in the visible range, with most emitting in the infrared region. This suggests that while doping can effectively tune the emission properties of GQDs, achieving desired visible emissions may require careful selection of both dopant type and concentration.

The comprehensive dataset generated, including emission energies and molecular structures,

provides a valuable resource for further theoretical and experimental exploration. This work offers critical insights into the design of GQDs for applications requiring specific optical properties, such as in optoelectronics, bioimaging, and sensing. Moreover, the systematic trends identified here can serve as a guide for future experimental efforts to optimize GQD properties with minimal trial and error, paving the way for the development of next-generation materials with tailored photonic characteristics.

V. ACKNOWLEDGEMENT

Ş.Ö. is supported by TÜBİTAK under grant no. 120F354. Computing resources used in this work were provided by the National Center for High Performance Computing of Türkiye (UHeM) under grant no. 1007872020 and TUBITAK ULAKBIM, High Performance and Grid Computing Center (TRUBA).

-
- [1] Mahto, B., Mahanty, B., Hait, S. & Hussain, S. A review of coal-based carbon and graphene quantum dots: synthesis, properties, and applications. *Materials Science and Engineering: B* **304**, 117386 (2024).
 - [2] Reckmeier, C. J., Schneider, J., Susha, A. S. & Rogach, A. L. Luminescent colloidal carbon dots: optical properties and effects of doping. *Optics Express* **24**, A312 (2016).
 - [3] Kovalchuk, A., Huang, K., Xiang, C., Martí, A. A. & Tour, J. M. Luminescent polymer composite films containing coal-derived graphene quantum dots. *ACS Applied Materials & Interfaces* **7**, 26063–26068 (2015).
 - [4] Deng, J.-P., Chen, W.-H., Chiu, S.-P., Lin, C.-H. & Wang, B.-C. Edge-termination and core-modification effects of hexagonal nanosheet graphene. *Molecules* **19**, 2361–2373 (2014).
 - [5] Du, T. *et al.* Role of functionalization in the fluorescence quantum yield of graphene quantum dots. *Applied Physics Letters* **122** (2023).
 - [6] Mandal, B., Sarkar, S. & Sarkar, P. Exploring the electronic structure of graphene quantum dots. *Journal of Nanoparticle Research* **14**, 1317 (2012).
 - [7] Tian, P., Tang, L., Teng, K. & Lau, S. Graphene quantum dots from chemistry to applications. *Materials Today Chemistry* **10**, 221–258 (2018).
 - [8] Sun, H., Wu, L., Wei, W. & Qu, X. Recent advances in graphene quantum dots for sensing. *Materials Today* **16**, 433–442 (2013).
 - [9] Yuan, F. *et al.* Engineering triangular carbon quantum dots with unprecedented narrow bandwidth emission for multicolored leds. *Nature Communications* **9**, 2249 (2018).

- [10] Wang, K. *et al.* A fluorescent probe for selective detection of Fe^{3+} by using a self-assembled nitrogen-doped carbon quantum dots-3,4,9,10-perylenetetracarboxylic acid composite. *Ionics* **27**, 4907–4916 (2021).
- [11] Singh, J. *et al.* Highly fluorescent carbon dots derived from mangifera indica leaves for selective detection of metal ions. *Science of The Total Environment* **720**, 137604 (2020).
- [12] Zou, C. *et al.* Carbon-dot and quantum-dot-coated dual-emission core–satellite silica nanoparticles for ratiometric intracellular Cu^{2+} imaging. *Analytical Chemistry* **88**, 7395–7403 (2016).
- [13] Omer, K. M., Tofiq, D. I. & Ghafoor, D. D. Highly photoluminescent label free probe for chromium (ii) ions using carbon quantum dots co-doped with nitrogen and phosphorous. *Journal of Luminescence* **206**, 540–546 (2019).
- [14] Saikia, M., Das, T. & Saikia, B. K. A novel rapid synthesis of highly stable silver nanoparticle/carbon quantum dot nanocomposites derived from low-grade coal feedstock. *New Journal of Chemistry* **46**, 309–321 (2022).
- [15] Li, H. *et al.* Synthesis, modification strategies and applications of coal-based carbon materials. *Fuel Processing Technology* **230**, 107203 (2022).
- [16] Lim, S. Y., Shen, W. & Gao, Z. Carbon quantum dots and their applications. *Chemical Society Reviews* **44**, 362–381 (2015).
- [17] Lee, S.-Y. & Mahajan, R. L. A facile method for coal to graphene oxide and its application to a biosensor. *Carbon* **181**, 408–420 (2021).
- [18] Cui, Y. *et al.* Graphene quantum dots/carbon nitride heterojunction with enhanced visible-light driven photocatalysis of nitric oxide: An experimental and dft study. *Carbon* **191**, 502–514 (2022).
- [19] Xu, D., Lin, Q. & Chang, H. Recent advances and sensing applications of carbon dots. *Small Methods* **4** (2020).
- [20] Wang, C. *et al.* Carbon quantum dots-ag nanoparticle complex as a highly sensitive “turn-on” fluorescent probe for hydrogen sulfide: A dft/td-dft study of electronic transitions and mechanism of sensing. *Sensors and Actuators B: Chemical* **264**, 404–409 (2018).
- [21] Yang, M., Lian, Z., Si, C. & Li, B. Revealing the role of nitrogen dopants in tuning the electronic and optical properties of graphene quantum dots <i>via</i> a td-dft study. *Physical Chemistry Chemical Physics* **22**, 28230–28237 (2020).
- [22] Liu, Y. *et al.* Red emission b, n, s-co-doped carbon dots for colorimetric and fluorescent dual mode detection of Fe^{3+} ions in complex biological fluids and living cells. *ACS Applied Materials & Interfaces* **9**, 12663–12672 (2017).
- [23] Budak, E., Aykut, S., Paşaoğlu, M. E. & Ünlü, C. Microwave assisted synthesis of boron and nitrogen rich graphitic quantum dots to enhance fluorescence of photosynthetic pigments. *Materials Today Communications* **24**, 100975 (2020).
- [24] Li, F. *et al.* Mg/n double doping strategy to fabricate extremely high luminescent carbon dots for bioimaging. *RSC Adv.* **4**, 3201–3205 (2014).

- [25] Parvin, N. & Mandal, T. K. Dually emissive p,n-co-doped carbon dots for fluorescent and photoacoustic tissue imaging in living mice. *Microchimica Acta* **184**, 1117–1125 (2017).
- [26] Budak, E. & Ünlü, C. Boron regulated dual emission in b, n doped graphene quantum dots. *Optical Materials* **111**, 110577 (2021).
- [27] Miao, S. *et al.* Hetero-atom-doped carbon dots: Doping strategies, properties and applications. *Nano Today* **33**, 100879 (2020).
- [28] Redondo-Fernandez, G., Canga, J. C., Soldado, A., Encinar, J. R. & Costa-Fernandez, J. M. Functionalized heteroatom-doped carbon dots for biomedical applications: A review. *Analytica Chimica Acta* **1284**, 341874 (2023).
- [29] Xu, Q. *et al.* Heteroatom-doped carbon dots: synthesis, characterization, properties, photoluminescence mechanism and biological applications. *Journal of Materials Chemistry B* **4**, 7204–7219 (2016).
- [30] Sohal, N., Maity, B. & Basu, S. Recent advances in heteroatom-doped graphene quantum dots for sensing applications. *RSC Advances* **11**, 25586–25615 (2021).
- [31] Runge, E. & Gross, E. K. U. Density-functional theory for time-dependent systems. *Physical Review Letters* **52**, 997–1000 (1984).
- [32] Sarkar, R., Boggio-Pasqua, M., Loos, P.-F. & Jacquemin, D. Benchmarking td-dft and wave function methods for oscillator strengths and excited-state dipole moments. *Journal of Chemical Theory and Computation* **17**, 1117–1132 (2021).
- [33] Wang, X., Gao, S., Zhao, M. & Marom, N. Benchmarking time-dependent density functional theory for singlet excited states of thermally activated delayed fluorescence chromophores. *Physical Review Research* **4**, 033147 (2022).
- [34] Wazzan, N., Irfan, A. & Fagieh, T. M. Dft investigation of graphene quantum dot-ixora floral natural dye (gqd-ndix) nanocomposites as visible light harvesters in dye-sensitized solar cells. *Journal of Molecular Liquids* **360**, 119531 (2022).
- [35] Jabed, M. A., Zhao, J., Kilin, D. & Yu, T. Understanding of light absorption properties of the n-doped graphene oxide quantum dot with td-dft. *The Journal of Physical Chemistry C* **125**, 14979–14990 (2021).
- [36] Şener Özönder, Ünlü, C., Güleriyüz, C. & Trabzon, L. Doped graphene quantum dots uv–vis absorption spectrum: A high-throughput tddft study. *ACS Omega* **8**, 2112–2118 (2023).
- [37] Schumacher, S. Photophysics of graphene quantum dots: Insights from electronic structure calculations. *Physical Review B* **83**, 081417 (2011).
- [38] Zhao, M., Yang, F., Xue, Y., Xiao, D. & Guo, Y. A time-dependent dft study of the absorption and fluorescence properties of graphene quantum dots. *ChemPhysChem* **15**, 950–957 (2014).
- [39] Liu, Z. *et al.* Theoretical investigation of red-shifted emission of graphitic boron doping in graphene quantum dots. *Diamond and Related Materials* **142**, 110815 (2024).
- [40] Bannwarth, C. *et al.* Extended tight-binding quantum chemistry methods. *WIREs Comput. Mol. Sci.* **11**, e01493 (2020).

- [41] Bannwarth, C., Ehlert, S. & Grimme, S. Gfn2-xtb—an accurate and broadly parametrized self-consistent tight-binding quantum chemical method with multipole electrostatics and density-dependent dispersion contributions. *Journal of Chemical Theory and Computation* **15**, 1652–1671 (2019).
- [42] Frisch, M. J. *et al.* Gaussian16 Revision C.01 (2016). Gaussian Inc. Wallingford CT.
- [43] Becke, A. D. Density-functional thermochemistry. III. The role of exact exchange. *The Journal of Chemical Physics* **98**, 5648–5652 (1993).
- [44] Lee, C., Yang, W. & Parr, R. G. Development of the colle-salvetti correlation-energy formula into a functional of the electron density. *Phys. Rev. B* **37**, 785–789 (1988).
- [45] Vosko, S. H., Wilk, L. & Nusair, M. Accurate spin-dependent electron liquid correlation energies for local spin density calculations: a critical analysis. *Canadian Journal of Physics* **58**, 1200–1211 (1980).
- [46] Dill, J. D. & Pople, J. A. Self-consistent molecular orbital methods. xv. extended gaussian-type basis sets for lithium, beryllium, and boron. *J. Chem. Phys.* **62**, 2921–2923 (1975).
- [47] Ditchfield, R., Hehre, W. J. & Pople, J. A. Self-consistent molecular-orbital methods. ix. an extended gaussian-type basis for molecular-orbital studies of organic molecules. *J. Chem. Phys.* **54**, 724–728 (1971).
- [48] Francl, M. M. *et al.* Self-consistent molecular orbital methods. xxiii. a polarization-type basis set for second-row elements. *J. Chem. Phys.* **77**, 3654–3665 (1982).
- [49] Frisch, M. J. *et al.* Gaussian 09 revision e.01. Gaussian, Inc., Wallingford, CT, 2009.
- [50] Gordon, M. S., Binkley, J. S., Pople, J. A., Pietro, W. J. & Hehre, W. J. Self-consistent molecular-orbital methods. 22. small split-valence basis sets for second-row elements. *J. Am. Chem. Soc.* **104**, 2797–2803 (1982).
- [51] Hariharan, P. C. & Pople, J. A. The influence of polarization functions on molecular orbital hydrogenation energies. *Theor. Chim. Acta* **28**, 213–222 (1973).
- [52] Hehre, W. J., Ditchfield, R. & Pople, J. A. Self-consistent molecular orbital methods. xii. further extensions of gaussian-type basis sets for use in molecular orbital studies of organic molecules. *J. Chem. Phys.* **56**, 2257–2261 (1972).
- [53] Improta, R., Scalmani, G., Frisch, M. J. & Barone, V. Toward effective and reliable fluorescence energies in solution by a new state specific polarizable continuum model time dependent density functional theory approach. *The Journal of Chemical Physics* **127**, 074504 (2007).